On the ice-nucleating potential of warm hydrometeors in mixed-phase clouds

Michael Krayer[1], Agathe Chouippe[1,a], Markus Uhlmann[1], Jan Dušek[2], and Thomas Leisner[3]

[1]Institute for Hydromechanics, Karlsruhe Institute of Technology (KIT), Karlsruhe, Germany
[2]ICube, Fluid Mechanics Group, Université de Strasbourg, Strasbourg, France
[3]Institute of Meteorology and Climate Research, Atmospheric Aerosol Research Department, Karlsruhe Institute of Technology (KIT), Eggenstein-Leopoldshafen, Germany
[a]now at: ICube, Fluid Mechanics Group, Université de Strasbourg, Strasbourg, France

Correspondence: Michael Krayer (michael.krayer@kit.edu)

Abstract. The question whether or not the presence of warm hydrometeors in clouds may play a significant role in the nucleation of new ice particles has been debated for several decades. While the early works of Fukuta and Lee (1986) and Baker (1991) indicated that it might be irrelevant, the more recent study of Prabhakaran et al. (2019) suggested otherwise. In this work, we are aiming to quantify the ice-nucleating potential using high-fidelity flow simulation techniques around a single

5   hydrometeor and use favorable considerations to upscale the effects to a collective of ice particles in clouds. While we find that ice nucleation may be enhanced in the vicinity of a warm hydrometeor by several orders of magnitude and that the affected volume of air is much larger than previously estimated, it is very unlikely that this effect alone causes the rapid enhancement of ice nucleation observed in some types of clouds, mainly due to the low initial volumetric ice concentration. Nonetheless, it is suggested to implement this effect into existing cloud models in order to investigate second-order effects such as ice nucleus

10   preactivation or enhancement after the onset of glaciation.

1   Introduction

The formation of hydrometeors in clouds is of great importance for the prediction of weather and cloud electrification, as well as for the hydrological cycle, and thus, eventually for the evolution of climate. However, despite its relevance and great research effort over the past decades, many aspects remain poorly understood. One such puzzle is the discrepancy between

15   the concentration of ice particles and that of available ice nuclei in airborne observations by several orders of magnitude (Pruppacher and Klett, 2010) which has been observed for various cloud types (Koenig, 1963; Auer et al., 1969; Hobbs, 1969; Hobbs and Rangno, 1985; Mossop, 1985; Hogan et al., 2002). This phenomenon has been termed *ice enhancement* and various mechanisms which amplify primary ice nucleation have been proposed to explain the observed surplus in ice particles (Field et al., 2016) .

20   The most promising class of enhancement mechanisms is the so-called *secondary ice production* (SIP), where new ice is formed from preexisting ice particles. Commonly accepted SIP include rime-splintering (Hallett and Mossop, 1974), fragmentation of ice (Vardiman, 1978; Takahashi et al., 1995; Bacon et al., 1998) and freezing drops (Hobbs and Alkezweeny,

1968). Most of these mechanisms have been implemented into cloud models with explicit ice microphysics (see Field et al. (2016) for a recent overview), which, however, are not capable of satisfactorily explaining the large amount of ice particles in
25 observations. Further mechanisms have been proposed in the past whose relative importance is still to be evaluated.

While studying the effect of supersaturation on primary ice formation, Gagin (1972) proposed several mechanisms which locally produce high values of supersaturation, and thus, regions of significantly enhanced nucleation activity. He suggested that freezing hydrometeors, which attain higher temperatures than the surrounding air due to the release of latent heat, may cause transient supersaturation by simulateneous evaporation and heat transfer and linked it to the observation of satellite drops
30 which have previously been observed experimentally during the freezing of supercooled droplets by Dye and Hobbs (1968). This hypothesis was corroborated by Nix and Fukuta (1974), who investigated numerically the transient freezing process of an isolated droplet.

Another phenomenon which leads to localized supersaturation around hydrometeors is the riming process of ice particles in mixed-phase clouds with high liquid-water content (Gagin, 1972). Here, sufficiently large ice particles collect super-
35 cooled droplets from their surroundings, which then accumulate on its surface and subsequently freeze, leading to similar non-equilibrium conditions as observed for the freezing drop. The supersaturation around a riming ice particle has been investigated numerically by Fukuta and Lee (1986) assuming steady conditions. Indeed, they found that the air in the vicinity of a warm ice particle can be highly supersaturated, while the magnitude and spatial extent strongly increase with increasing difference in surface to ambient temperature. However, even at low cloud temperatures, the supersaturated regions do not extend
40 far away from the hydrometeor in their simulations, which led to the conclusion of Rangno and Hobbs (1991) that the overall ice enhancement is likely to be negligible.

While the previously mentioned studies focused on the quantification of the supersaturation field, Baker (1991) attempted to quantify the actual effect on ice enhancement around warm hydrometeors. He concluded that, although significant ice enhancement factors appear to be possible, the affected air mass seems to be too small to substantially contribute to the
45 explanation of the discrepancy between ice crystal and ice nucleus concentrations.

Recently, the potential of hail and rain to nucleate droplets has gained new attention when Prabhakaran et al. (2017) observed condensation in the wake of cold droplets in a moist convection apparatus. In their experiment, a pressurized mixture of sulfur hexafluoride/helium was used and operating conditions were chosen such that slight supersaturations led to homogeneous condensation, which could indeed be observed in the wake of larger falling droplets. However, their results can only be
50 qualitatively transfered to Earth's atmosphere mainly due to the difference in primary nucleation mechanism. Moreover, the mechanism to create supersaturation is different from the previously discussed one in the sense that the droplets are colder than the surrounding air.

To overcome these shortcomings, Prabhakaran et al. (2019) conducted a similar laboratory experiment using moist air which has been seeded with aerosol particles as an operating medium to investigate heterogeneous nucleation in the wake of a warm
55 falling droplet. Again, significant nucleation was observed in the wake of the falling hydrometeor. While the extent of wake-induced nucleation has not been quantified, the affected volume of air appears to be significantly larger than the predictions of Fukuta and Lee (1986) and Baker (1991) were suggesting. This discrepancy might be related to the strong assumptions on the

flow made in these early works, which neglect important features of the wake of falling objects that are nowadays accessible to numerical simulations (Johnson and Patel, 1999; Bouchet et al., 2006; Zhou and Dušek, 2015). In particular, it has been shown that both unsteadiness and vortical structures of the flow strongly affect the temperature and vapor concentration in the vicinity and far downstream of a falling sphere (Bagchi et al., 2001; de Stadler et al., 2014), and thus strongly affect the distribution of supersaturation around hydrometeors (Chouippe et al., 2019).

In Chouippe et al. (2019), we presented a framework for high-fidelity numerical simulations of heat and mass transfer around a falling ice particle which is not in thermal equilibrium with its surroundings. Even though the focus was predominantly set towards several methodological questions, it was shown qualitatively that the local supersaturation differs strongly from the simpler considerations of Fukuta and Lee (1986).

The present work aims to revisit the details of the supersaturation field around an idealized falling hydrometeor and to quantify the volume of air which is affected by the presence of hydrometeors. Furthermore, it is yet to be evaluated how significant meteor-induced enhancement of ice nucleation is in clouds (Korolev et al., 2020), and therefore, we attempt to link our results to heterogeneous nucleation of aerosol particles.

2 Methodology

In order to assess the spatial structure of supersaturation around hydrometeors, knowledge on the flow around it is essential. This is not an easy task, since the features of the flow may strongly depend on parameters such as the size, shape and surface properties of the hydrometeor, which typically vary substantially, especially if ice particles are concerned.

In this work we utilize the numerical framework previously presented in Chouippe et al. (2019) and model the hydrometeor as a sphere with constant diameter D, constant surface temperature T_p and a constant vapor pressure $e_{v,p}$ at its surface. The latter is determined by the assumption of local equilibrium at the surface, and thus, corresponds to the saturation vapor pressure $e_{sat,j}$ at T_p. Here, j denotes the phase of water on the surface of the hydrometeor, where subscript "i" will be used to denote the solid phase and "w" to denote the liquid phase.

The boundary conditions for the heat and mass transfer problem are motivated by the conditions expected for riming ice particles in the wet-growth regime. A surface temperature of $T_p = 0\,°C$ is assumed, i.e. the surface of the ice sphere is warmer than the local cloud temperature, since the latter is generally below the freezing point in mixed-phase clouds. Please note that at this surface temperature the equilibrium vapor pressure with respect to both the liquid and solid phase coincide, and hence, no assumptions on the phase at the surface have to be made. Since the actual riming process is not modelled explicitly, but only enters through the boundary conditions of the heat and mass transfer problem, the results of this work are more general and can in principle be applied to any configuration which contains a mechanism leading to a warm hydrometeor, such as a freezing droplet or rapid decreases in cloud temperature.

One of the key parameters for the investigation of wake-induced ice nucleation is the distribution of the saturation ratio

$$S_j(e,T) = e/e_{sat,j}(T),\qquad(1)$$

90   where e denotes the local vapor pressure. A parametrization of $e_{sat,j}$ with respect to temperature for both phase equilibria in the temperature range of interest is adopted from Murphy and Koop (2005). The spatial distribution of S_j can then be reconstructed from the temperature field T and the vapor concentration n_v, which are governed by the transport equations

$$\frac{\partial T}{\partial t} + \boldsymbol{u} \cdot \boldsymbol{\nabla} T = \mathcal{D}_T \boldsymbol{\nabla}^2 T, \tag{2}$$

$$\frac{\partial n_v}{\partial t} + \boldsymbol{u} \cdot \boldsymbol{\nabla} n_v = \mathcal{D}_{n_v} \boldsymbol{\nabla}^2 n_v, \tag{3}$$

95   where $\mathcal{D}_T$ and $\mathcal{D}_{n_v}$ denote the heat and vapor diffusivities and $\boldsymbol{u} = (u, v, w)^T$ is the velocity field of the surrounding air. The partial pressure of water is linked to these transported quantities by

$$e = n_v / k_b T, \tag{4}$$

where k_b is Boltzmann's constant. Even though the diffusivities of both vapor and heat are similar in magnitude, it was shown by Chouippe et al. (2019) that assuming equal diffusivities leads to an underestimation of the saturation ratio, and hence, both
100 equations will be treated separately.

Under the boundary conditions described earlier, Eq. (2) leads to an outward heat flux, because the surface temperature of the hydrometeor is higher than that of its surrounding. Furthermore, at $T_p = 0\,^\circ\mathrm{C}$ the vapor concentration at the meteor's surface is generally higher than in the ambient, since latter is assumed to be in equilibrium with the liquid phase at the corresponding cloud temperature $T_\infty < T_p$ due to the presence of droplets in mixed-phase clouds, i.e. $e_\infty = e_{sat,w}(T_\infty)$. This results in
105 an outward vapor flux, and hence, the hydrometeor will also evaporate. It is therefore of primary importance to resolve the temporal and spatial variations of both temperature and concentration fields.

In Chouippe et al. (2019) we have shown that buoyant forces due to density variations within the fluid phase caused by variations in temperature and concentration are negligible at the parameter point of interest. The flow can then be approximated by the incompressible Navier-Stokes equations,

110
$$\boldsymbol{\nabla} \cdot \boldsymbol{u} = 0, \tag{5}$$

$$\frac{\partial \boldsymbol{u}}{\partial t} + (\boldsymbol{u} \cdot \boldsymbol{\nabla})\boldsymbol{u} = -\frac{1}{\rho_f}\boldsymbol{\nabla} p + \nu \boldsymbol{\nabla}^2 \boldsymbol{u}, \tag{6}$$

where p denotes the hydrodynamic pressure, ρ_f the density and ν the kinematic viscosity of the fluid. The flow is driven by the falling motion of the hydrometer, which is assumed to be moving with a constant velocity $\boldsymbol{v}_p$ equal to its terminal velocity v_T, i.e.

115
$$\boldsymbol{v}_p = -v_T \boldsymbol{e}_z, \tag{7}$$

where $\boldsymbol{e}_z$ is the unit vector in the z-direction. The fluid ahead of the hydrometeor is assumed to be at rest. This setup is equivalent to a system with a fixed sphere positioned in an upcoming flow, which differs from that of a freely falling mobile sphere in the sense that fluctuations in $\boldsymbol{v}_p$ are not permitted. The necessity to account for these variations has been discussed in Chouippe et al. (2019) and it was found that it has little influence in the present context.

The Navier-Stokes and scalar transport equations are solved numerically in non-dimensional form. In particular lengths are scaled by the particle diameter D, velocity components by the terminal velocity v_T and the scalar transport equations are formulated in terms of

$$\tilde{T} = (T - T_\infty)/(T_p - T_\infty), \tag{8}$$

$$\tilde{n}_v = (n_v - n_{v,\infty})/(n_{v,p} - n_{v,\infty}), \tag{9}$$

which has the advantage, that various dimensional boundary conditions, e.g. various values of T_∞, can be studied in post-processing from a single simulation run. Under the simplifications stated, the non-dimensional problem can be parametrized by the Reynolds number, $Re = |\boldsymbol{v}_p| D/\nu$, the Prandtl number, $Pr = \nu/\mathcal{D}_T$, and the Schmidt number, $Sc = \nu/\mathcal{D}_{n_v}$. While the Reynolds number is varied up to a value of $Re = 600$, the Prandtl and Schmidt numbers are set, respectively, to values of $Pr = 0.72$ and $Sc = 0.63$ in this study, which correspond to representative values expected for humid air in the temperature range of interest.

The numerical method employed is based on the method of Jenny and Dušek (2004), which has been used by e.g. Kotouč et al. (2008) and Chouippe et al. (2019) to simulate heat and mass transfer around spherical particles. It relies on a spectral/spectral-element discretiztion of the Navier-Stokes equations (Eq. 5,6) coupled to the transport of heat and mass (Eq. 2,3). The spherical particle is placed at the origin of a cylindrical domain Ω. On the surface of the particle impermeability and no-slip boundary conditions are imposed, while the scalar fields are subject to the constant Dirichlet boundary conditions $\tilde{T} = \tilde{n}_v = 1$. At the upstream boundary of the simulation domain, a uniform velocity condition and $\tilde{T} = \tilde{n}_v = 0$ are enforced, while the downstream boundary is subject to zero-gradient boundary conditions for velocity as well as the scalars. The lateral boundaries are stress-free with zero-gradient boundary conditions for the scalars and zero pressure is imposed. The axial-radial plane is decomposed using the spectral element method of Patera (1984), while the homogeneous azimuthal direction is treated using Fourier decomposition. The numerical mesh used in this work is shown in fig. 1. For the temporal integration a time splitting method is used which consists of an explicit third order Adams-Bashforth discretization for the advective terms and a first order fully implicit discretization of the diffusion terms (Rønquist, 1988).

In the vertical direction the domain has a total length of $62D$, where the inflow length is $12D$ and the outflow length $50D$ measured from the center of the sphere. The diameter of the domain is $16D$. The computational domain has therefore been extended in the rear of the sphere compared to our former simulations presented in Chouippe et al. (2019). In total, 463 two-dimensional elements, each containing $[6 \times 6]$ collocation points, have been distributed over the domain. The azimuthal Fourier series is truncated at the 7th mode. This resolution is comparable to our previous work and has been shown to give good results for the momentum, as well has heat and mass transfer. All relevant scales of the flow and the scalar fields are resolved.

For more details on the numerical framework, the reader is referred to the previous work of Chouippe et al. (2019).

3 Results

3.1 Hydrometeor wake regimes in clouds

The dynamics of the flow around spherical objects are, under the assumptions stated in the previous section, fully parametrized by the Reynolds number, which depends on the diameter and indirectly, through modulation of the terminal velocity, on the density of the hydrometeor. Depending on the Reynolds number value, various flow states emerge in the wake (Johnson and Patel, 1999; Jenny et al., 2004; Kotouč et al., 2009). At low values the wake is axisymmetric and steady. When the first critical value of the Reynolds number, $Re_{c,1} \approx 212$, is exceeded, the wake becomes oblique with respect to the falling direction (*steady oblique regime*) and only planar symmetry may be observed (Ghidersa and Dušek, 2000). At $Re_{c,2} \approx 273$ a second instability of Hopf type occurs (Ghidersa and Dušek, 2000), which leads to unsteady periodic vortex shedding, while planar symmetry is still maintained (*oscillating oblique regime*). Eventually the vortex shedding becomes chaotic at $Re_{c,3} \approx 360$ (Ormières et al., 1999) and all instantaneous symmetries are lost (*chaotic regime*). The listed regimes differ significantly in their ability to transfer heat and mass (Chouippe et al., 2019), and thus, different characteristics in producing local supersaturation are to be expected.

In order to estimate the distribution of ice particle wake regimes in clouds, we adopt the size distribution of Marshall and Palmer (1948),

$$N = N_0 \exp\left(-\lambda D\right), \tag{10}$$

where N is the number concentration density of hydrometeors per unit volume of air and N_0, λ are model parameters. Equation (10) has originally been developed for raindrops, however, its validity for sufficiently large ice particles has been demonstrated by Passarelli (1978); Houze et al. (1979); Gordon and Marwitz (1984); Herzegh and Hobbs (1985); Patade et al. (2015) for various types of natural clouds. The values of the model parameters N_0, λ are usually obtained by airborne measurements and given as functions of the cloud temperature. One such parametrization is provided by Houze et al. (1979) for frontal clouds within a temperature range from $-42°C$ to $+6°C$, which will be used in the following for the size distribution of primary ice and is given by the constitutive equations

$$N_0(T) = 5.5 \cdot 10^6 \exp\left(-0.09T\right) \mathrm{m}^{-4}, \tag{11}$$

$$\lambda(T) = 9.6 \cdot 10^{-1} \exp\left(-0.056T\right) \mathrm{mm}^{-1}, \tag{12}$$

where T denotes the cloud temperature in $°C$. For this cloud type, ice enhancement has been previously reported in the presence of riming ice particles (Hogan et al., 2002). Even though it is known that the number density of ice particles of sub-millimeter size might deviate significantly from Eq. (10) in a sub-exponential or super-exponential manner (Passarelli, 1978), depending on cloud conditions, we assume that Eq. (10) holds nonetheless for all ice particle sizes for the sake of simplicity.

For reasons explained in section 3.3, our quantity of interest is not the number concentration, but rather the volume fraction ϕ of hydrometeors in clouds, which can be obtained by integrating the corresponding moment of the Marshall-Palmer

distribution, i.e.

$$\phi = \int_0^\infty \frac{\pi D^3}{6} N_0 \exp\left(-\lambda D\right) \mathrm{d}D. \tag{13}$$

In order to determine the wake regimes from the size distribution, the terminal velocity needs to be approximated as a function of the ice particle diameter, and hence, further assumptions on the density of the ice particles have to be made. For graupel

185 particles, the density may take values which range between $0.05\,\mathrm{g\,cm^{-3}}$ and $0.89\,\mathrm{g\,cm^{-3}}$, depending on growth conditions and history (Pruppacher and Klett, 2010). For our estimation we choose a value of $0.6\,\mathrm{g\,cm^{-3}}$, as we are primarily concerned with ice particles in the wet-growth mode, which typically constitute the upper end of the density range. Using this value and the empirical drag law of Schiller and Naumann (1933), the critical diameters for regime transition are calculated from the critical Reynolds numbers. The total solid volume fraction can then be subdivided into the contributions by ice particles with a certain

190 wake regime, i.e.

$$\phi \equiv \sum_j \phi_j = \sum_j \int_{D_{j,\mathrm{min}}}^{D_{j,\mathrm{max}}} \frac{\pi D^3}{6} N_0 \exp\left(-\lambda D\right) \mathrm{d}D, \tag{14}$$

where the index j denotes one of the four wake regimes (steady axisymmetric; steady oblique; oscillating oblique; chaotic) and $D_{j,\mathrm{min}}, D_{j,\mathrm{max}}$ the corresponding lower/upper limit for the hydrometeor diameter to be in this regime.

Figure 2 shows the estimated volume fraction of frozen hydrometeors in clouds as a function of cloud temperature. The

195 values are typically smaller than 10^{-5} and decrease exponentially with decreasing temperature. When comparing the various regimes, it can be observed that the largest contributions generally stem from hydrometeors in the axisymmetric or chaotic regime. This becomes especially clear when looking at the relative contribution of ϕ_j to the total volume fraction ϕ as shown in fig. 3. As can be seen, more than 80% of ice particles (by volume) exhibit one of these two wake regimes. Chaotic wakes are dominant at temperatures close to the freezing point, while axisymmetric wakes dominate when the temperature is very low.

200 We will therefore focus solely on the axisymmetric and chaotic regimes in the following.

3.2 Supersaturation in the wake of hydrometeors

We now examine the saturation profiles in the wake of hydrometeors in the two regimes of interest. Figure 4 shows isocontours of supersaturation w.r.t. ice, defined as $s_i = S_i - 1$, for two different values of the Reynolds number, namely $Re = 75$, which lies within the axisymmetric regime, and $Re = 600$ in the chaotic wake regime. As ambient temperature, a value of $T_\infty = -30°\mathrm{C}$

205 was adopted, because this roughly corresponds to the cloud temperature where the two regimes are of equal significance (cf. fig. 3). Since the ambient fluid is already supersaturated w.r.t. ice, the threshold of the isocontours is given as an excess to the value in the ambient and we define the excess supersaturation as

$$\tilde{s} \equiv s - s_\infty. \tag{15}$$

At $Re = 75$, the flow is steady, and thus, so is the supersaturation field. In the chaotic regime, the flow is characterized by

210 time-dependent vortex shedding from the ice particle's boundary layer, and therefore excess supersaturation appears intermit-

tently. In both regimes, significant excess supersaturation w.r.t. the ambient can be observed far downstream and the volume of air which is affected by the wake is by far larger than the volume of the meteor. This can be seen more clearly when averaging the fields in the azimuthal direction, which is statistically homogeneous for both cases, as well as in time for the unsteady flow. The averaged excess supersaturation w.r.t. ice is shown in fig. 5 for both cases. The saturation profiles differ substantially from

215 the ones obtained by Fukuta and Lee (1986) for similar boundary conditions and Reynolds number. This is presumably due to their strong simplification of potential flow, which is incapable of reproducing the boundary layer and the flow in the wake of the ice particle correctly. This indeed leads to strong modifications in the distribution of supersaturated regions. Regions of high vapor content and relatively low temperatures, i.e. supersaturated regions, which are created in the mixing layer close to the riming particle are transported further downstream by the detaching vortices in the chaotic regime. This effect does not occur

220 in the simulations of Fukuta and Lee (1986), who observed a complete decay of supersaturation to the inflow value within a distance of approximately $2.5D$ downstream of the ice particle for $T_\infty = -30°C$ while fig. 5 clearly indicates that regions with $\tilde{s}_i > 0$ may be observed at distances more than $50D$ from the rear at this temperature.

In order to compare the induced supersaturation for different values of T_∞ and in between different regimes, we compute the time-averaged volume of air which is supersaturated above a given threshold,

$$225 \quad V_s(s^*) \equiv \frac{1}{\tau} \int\limits_0^\tau \int\limits_\Omega H(s(\boldsymbol{x},t) - s^*) \, \mathrm{d}\Omega \, \mathrm{d}t, \tag{16}$$

where V_s is the superaturated volume, s^* the corresponding threshold and H the Heaviside step function. Figure 6 shows this quantity normalized by the volume of the ice particle as a function of the threshold. It can be seen, that in the axisymmetric regime, the supersaturated volume is generally larger than in the chaotic regime. This is caused by the enhanced mixing properties of the vortical wake structures in the latter case, which lead to a faster decay of the scalar field.

230 For both regimes, the range of observed values of supersaturation is similar. In fact, differences in range may only occur due to the distinct diffusivities of the temperature and water vapor fields, which indeed lead to subsaturations in the chaotic regime in some parts of the flow. While the range can be estimated reasonably well using simple mixing arguments (Chouippe et al., 2019), we observe that the highest values of supersaturation only occur in a very confined portion of the wake. However, if the temperature difference between the ambient and the ice particle is sufficiently high, a strong excess in supersaturation

235 compared to the ambient value may occur in a volume comparable to the size of the meteor, if no mechanism for depletion is considered. This excess may be as high as 270% at a temperature difference of 40K. For all values of T_∞ the volume of air which is affected by the wake-induced supersaturation is of the order of 10^3 particle volumes.

3.3 Ice enhancement due to meteor wakes

Our spatially resolved data allows us, for the first time to our knowledge, to quantify the significance of wake-induced su-

240 persaturation on ice enhancement. Thus, in this section, we are now aiming to estimate how the nucleation of ice is affected by this excess in supersaturation. We therefore adopt the commonly used ice enhancement factor (e.g. Baker, 1991), which is defined as the ratio between the observed number concentration of ice nuclei (IN) and that expected for a reference state. For

our problem, it will be defined as

$$f_i \equiv \frac{N_{IN}\,(\text{with meteors})}{N_{IN}\,(\text{without meteors})}. \tag{17}$$

245   The IN number concentration N_{IN}, i.e. those aerosol particles which can be activated at a given supersaturation, is commonly approximated by a power-law in terms of the supersaturation w.r.t. ice,

$$N_{IN} = C s_i^\alpha \tag{18}$$

where C, α are constants depending on the aerosol composition (Huffman, 1973). For natural aerosols, the exponent α typically ranges between 3 and 8, where larger values are attributed to more polluted air masses, e.g. near metropolitan or industrial areas

250   (Pruppacher and Klett, 2010). We are aware that Eq. (18) is a very simplified approach to the problem and its validity might be debatable. In particular, it does not take into account the various characteristics of the different freezing modes, which are dependent on the temperature and supersaturation w.r.t. the liquid phase, nor the time scales of freezing, which might play an significant role in the microphysical view. The results should therefore only be regared as a first crude estimation on the importance of wake-induced ice enhancement in clouds.

255   Using Eq. (18), the local ice enhancement factor can be expressed as

$$f_i(\boldsymbol{x}) = \frac{\langle s_i^\alpha \rangle_t (\boldsymbol{x})}{s_{i,\infty}^\alpha}. \tag{19}$$

This quantity gives a quantitative measure on how much more ice is produced in the wake of the hydrometeor compared to the ambient under the limitations stated above. Figure 7 shows how the ice enhancement is distributed in the wake of a hydrometeor at $T_\infty = -30°$C for an exponent of $\alpha = 8$. At this parameter point, which can be considered as rather favorable, we observe

260   that f_i can locally reach extremely high values of the order of 10^4 in the near vicinity of the hydrometeor and significant values greater than 10 can still be observed in the far wake.

Using Eq. (19), the supersaturated volume can be expressed as a function of the ice enhancement factor in order to gain insight into the volumetric distribution of f_i. Figure 8 shows the distributions for $\alpha = 8$ and various temperatures in both wake regimes. The ice enhancement is generally higher in the axisymmetric regime than in the chaotic regime. Please note, that for a

265   more precise analysis of this behavior, the actual flow-driven distribution of aerosol particles in the wake should be considered. Depending on the flow dynamics, ice nucleating particles might accumulate in the wake or be expelled from it (Homann and Bec, 2015), which might have a non-negligible impact on ice enhancement. However, the consideration of aerosol dynamics is outside the scope of the present work.

We therefore conclude that the wake of a hydrometeor may act as a site of increased nucleation activity, and that the volume

270   in which this increased activity occurs is much larger than the volume of the hydrometeor itself. This conclusion is consistent with recent experimental results of Prabhakaran et al. (2019) who observed nucleation of water droplets and ice particles in the wake of a hot drop under cold conditions with a temperature difference comparable to the one presented in fig. 7.

In order to assess the significance of the wake effect in clouds, a global ice enhancement factor needs to be computed, which takes into account the spatial distribution of f_i obtained by the numerical simulations, as well as the volumetric ice concentra-

275   tion. We define a control volume $\mathcal{V}$ within a cloud which is sufficiently large such that the hydrometeor size distribution follows

Eq. (10), but sufficiently small such that the saturation field is uniform (with a value of $s_{i,\infty}$) if no hydrometeor is present. The volume-averaged ice enhancement within this control volume is given by

$$\langle f_i \rangle_{\mathcal{V}} = \frac{\int_{\mathcal{V}} (f_i(\boldsymbol{x}) - 1)\, \mathrm{d}\mathcal{V}}{\int_{\mathcal{V}} \mathrm{d}\mathcal{V}} + 1, \tag{20}$$

where the integral has been decomposed into an excess contribution, which evaluates to zero outside of the wake, and a base
280 contribution, which is equal to unity. At sufficiently small volume fractions, the wakes of individual hydrometeors can be assumed to not interact, and hence, the integral in the enumerator of the first term in Eq. (20) can be expressed as a sum of contributions from independent hydrometeors, i.e.

$$\int_{\mathcal{V}} (f_i(\boldsymbol{x}) - 1)\, \mathrm{d}\mathcal{V} = \sum_{(k)} \int_{\Omega^{(k)}} (f_i(\boldsymbol{x}) - 1)\, \mathrm{d}\Omega^{(k)}, \tag{21}$$

where $\Omega^{(k)} \subseteq \mathcal{V}$ denotes the simulation domain scaled by the size of particle (k). By defining the excess ice enhancement per
285 meteor volume as

$$\tilde{f}_{i,\Omega^{(k)}} \equiv \frac{6}{\pi D^3} \int_{\Omega^{(k)}} (f_i(\boldsymbol{x}) - 1)\, \mathrm{d}\Omega^{(k)} \tag{22}$$

and assuming a continuous particle size distribution following Eq. (10), the volume-averaged ice enhancement within $\mathcal{V}$ can be expressed as

$$\langle f_i \rangle_{\mathcal{V}} = 1 + \int_0^\infty \tilde{f}_{i,\Omega} \frac{\pi D^3}{6} N_0 \exp\left(-\lambda D\right) \mathrm{d}D. \tag{23}$$

290 Since $\tilde{f}_{i,\Omega}$ is normalized by the volume of the ice particle, its value only depends on the flow field in non-dimensional form, i.e. the diameter dependency only enters through the value of the Reynolds number. For reasons of simplicity, we assume that $\tilde{f}_{i,\Omega}$ can be approximated for a given regime by the value determined for a single Reynolds number within that regime, which allows us to rewrite Eq. (23) in the simplified form

$$\langle f_i \rangle_{\mathcal{V}} = 1 + \sum_j \phi_j \tilde{f}_{i,\Omega_j}, \tag{24}$$

295 where ϕ_j is the volume fraction of meteors in regime j, as defined in Eq. (14), and $\tilde{f}_{i,\Omega_j}$ the value of the excess ice enhancement evaluated for a single value of the Reynolds number in that regime. As has already been discussed and shown in fig. 3, the axisymmetric and chaotic regimes contribute the most to the volume fraction. We therefore disregard the contribution of the two other regimes and adjust the threshold of regime transition accordingly.

$$\langle f_i \rangle_{\mathcal{V}} = 1 + \phi_{axi} \tilde{f}_{i,\Omega_{axi}} + \phi_{cha} \tilde{f}_{i,\Omega_{cha}} \tag{25}$$

300 Both ϕ_j and $\tilde{f}_{i,\Omega}$ are functions of ambient temperature, and thus the global ice enhancement factor originating from meteor wakes can be expressed as a function of cloud temperature. While the former decreases exponentially with decreasing temperature, the latter exhibits a strong increase leading to a counteracting effect. Furthermore, a large number of ice particles pertain to the axisymmetric regime for low temperatures, which is more favorable in terms of ice enhancement.

Please be aware that even though our aim is to quantify the wake-induced ice formation, the volume fraction of ice will be
regarded as constant. The reason for this is that the approach used in this study does not allow us to derive the time scales of
nucleation nor growth of newly created ice, and thus, the time-dependent coupling with the size distribution is inaccessible.
Therefore, the following considerations merely apply to the initial state of a possible rapid glaciation process.

Figure 9 shows the global ice enhancement factor as a function of ambient temperature for different values of α, the exponent
in Eq. (19). It can be seen that significant ice enhancement in the global sense only occurs at cloud temperatures below $-30°$C in
conjunction with high values of α. Even then, the enhancement is only marginal with $\langle f_i \rangle_{\mathcal{V}}$ being smaller than 8. We therefore
conclude that under typical cloud conditions hydrometeors do not directly lead to substantially enhanced ice nucleation on a
global scale.

Since the small volume fraction of ice is the limiting factor for ice enhancement on a global scale, we revisited our assumption
on the size distribution of ice particles in order to assess the sensitivity to the parametrization. Using the parametrization of
Heymsfield et al. (2002) for deep subtropical and tropical clouds, the ice volume fraction may be up to five times larger
at $T_\infty = -40°$C. However, at higher cloud temperatures, i.e. when the temperature difference between ice particles and the
ambient is moderate, the volume fraction is of the same order of magnitude as for the presented results, such that the conclusions
which have been drawn for frontal clouds also persist for this type of cloud.

4 Conclusion

In this study we have performed numerical simulations of momentum, heat and mass transfer around a warm hydrometeor in
order to assess the distribution of supersaturation in its wake, and moreover, the implications on ice nucleation enhancement.
Our simulation method is based on a body-conforming spectral/spectral-element discretization and all relevant scales of the
flow problem have been resolved. The hydrometeor is assumed to be of spherical shape and to possess a uniform surface tem-
perature of $0\,°$C, while the ambient temperature has been varied in a range between $-40\,°$C and $0\,°$C. The vapor concentration
is kept at saturation value with respect to ice at the particle surface, while it is saturated with respect to water in the ambient
(reflecting the presence of supercooled droplets). Two different values of the Reynolds number have been simulated in order
to capture the characteristics of the most relevant wake regimes, namely $Re = 75$, where the wake is steady and axisymmetric,
and $Re = 600$, where the wake is chaotic.

We found that significant values of supersaturation can be attained in the wake of warm hydrometeors, which persist long
enough to be observed at more than 50 particle diameters downstream of the meteor for sufficiently high differences in tem-
perature. The supersaturated volume of air exceeds the estimations by Fukuta and Lee (1986) by far, which is attributed to the
more accurate representation of the flow in the current study. This is an important observation since one of the key arguments
for disregarding wake-induced ice nucleation is the proclaimed small zone of influence (Baker, 1991).

Using a power-law approximation for the ice enhancement factor, we estimate that heterogeneous nucleation may be locally
enhanced by a factor comparable to the discrepancy between ice nuclei and ice particles observed in field measurements. This
enhancement increases strongly with decreasing cloud temperature and so does the affected volume of air, which is typically

of the order of several hundred particle diameters. However, due to the low volumetric concentration of ice in clouds, this local effect alone unlikely serves as an explanation for the global discrepancy, as arguments on upscaling have shown.

Nonetheless, it is conceivable that the present mechanism in conjunction with one (or several) secondary ice processes is of
340 greater relevance to the problem of ice formation. After a rapid glaciation process has been triggered, wake-induced nucleation might become significant, as the ice concentration then increases to considerable values. Futhermore, the question of whether or not wake-induced nucleation alone might trigger such a process has not been fully resolved yet, since the feedback on the size distribution of ice particles has been disregarded in this study. In order to assess this dynamical behavior, further time-resolved information on the (pre-)activation of ice nuclei in the wake currently appears to be necessary. This requires
345 microphysical modeling of the nucleation process and knowledge on the spatial distribution of aerosol particles downstream of the ice particle. A resulting parametrization may be added to existing cloud models with explicit microphysics in order to assess the evolution of the size distribution, and moreover, the relative significance of wake-induced nucleation in comparison to other secondary ice processes.

Data availability. The datasets are available upon request to the corresponding author.

350 *Author contributions.* TL and MU conceptualized the idea. JD provided the simulation code and mesh. MK conducted the simulations. MK, AC and MU post-processed the data and TL assisted in the interpretation of the results. MK prepared the manuscript and AC contributed to it. MU, AC, JD and TL revised the manuscript.

Competing interests. The authors declare that they have no conflict of interest.

Acknowledgements. The authors thank Alexei Kiselev for useful discussions. The simulations were partially performed at the Steinbuch
355 Centre for Computing in Karlsruhe and the computer resources, technical expertise and assistance provided by this center are thankfully acknowledged.

References

Auer, A. H., Veal, D. L., and Marwitz, J. D.: Observations of Ice Crystal and Ice Nuclei Concentrations in Stable Cap Clouds, Journal of the Atmospheric Sciences, 26, 1342–1343, https://doi.org/10.1175/1520-0469(1969)026<1342:OOICAI>2.0.CO;2, 1969.

360 Bacon, N. J., Swanson, B. D., Baker, M. B., and Davis, E. J.: Breakup of Levitated Frost Particles, Journal of Geophysical Research: Atmospheres, 103, 13 763–13 775, https://doi.org/10.1029/98JD01162, 1998.

Bagchi, P., Ha, M. Y., and Balachandar, S.: Direct Numerical Simulation of Flow and Heat Transfer From a Sphere in a Uniform Cross-Flow, Journal of Fluids Engineering, 123, 347–358, https://doi.org/10.1115/1.1358844, 2001.

Baker, B. A.: On the Nucleation of Ice in Highly Supersaturated Regions of Clouds, Journal of the Atmospheric Sciences, 48, 1904–1907,
365 https://doi.org/10.1175/1520-0469(1991)048<1905:OTNOII>2.0.CO;2, 1991.

Bouchet, G., Mebarek, M., and Dušek, J.: Hydrodynamic Forces Acting on a Rigid Fixed Sphere in Early Transitional Regimes, European Journal of Mechanics - B/Fluids, 25, 321–336, https://doi.org/10.1016/j.euromechflu.2005.10.001, 2006.

Chouippe, A., Krayer, M., Uhlmann, M., Dušek, J., Kiselev, A., and Leisner, T.: Heat and Water Vapor Transfer in the Wake of a Falling Ice Sphere and Its Implication for Secondary Ice Formation in Clouds, New Journal of Physics, 21, 043 043, https://doi.org/10.1088/1367-
370 2630/ab0a94, 2019.

de Stadler, M. B., Rapaka, N. R., and Sarkar, S.: Large Eddy Simulation of the near to Intermediate Wake of a Heated Sphere at Re=10,000, International Journal of Heat and Fluid Flow, 49, 2–10, https://doi.org/10.1016/j.ijheatfluidflow.2014.05.013, 2014.

Dye, J. E. and Hobbs, P. V.: The Influence of Environmental Parameters on the Freezing and Fragmentation of Suspended Water Drops, Journal of the Atmospheric Sciences, 25, 82–96, https://doi.org/10.1175/1520-0469(1968)025<0082:TIOEPO>2.0.CO;2, 1968.

375 Field, P. R., Lawson, R. P., Brown, P. R. A., Lloyd, G., Westbrook, C., Moisseev, D., Miltenberger, A., Nenes, A., Blyth, A., Choularton, T., Connolly, P., Buehl, J., Crosier, J., Cui, Z., Dearden, C., DeMott, P., Flossmann, A., Heymsfield, A., Huang, Y., Kalesse, H., Kanji, Z. A., Korolev, A., Kirchgaessner, A., Lasher-Trapp, S., Leisner, T., McFarquhar, G., Phillips, V., Stith, J., and Sullivan, S.: Secondary Ice Production: Current State of the Science and Recommendations for the Future, Meteorological Monographs, 58, 7.1–7.20, https://doi.org/10.1175/AMSMONOGRAPHS-D-16-0014.1, 2016.

380 Fukuta, N. and Lee, H. J.: A Numerical Study of the Supersaturation Field around Growing Graupel, Journal of the Atmospheric Sciences, 43, 1833–1843, https://doi.org/10.1175/1520-0469(1986)043<1833:ANSOTS>2.0.CO;2, 1986.

Gagin, A.: The Effect of Supersaturation on the Ice Crystal Production by Natural Aerosols, Journal de Recherches Atmosphériques, 6, 175–185, 1972.

Ghidersa, B. and Dušek, J.: Breaking of Axisymmetry and Onset of Unsteadiness in the Wake of a Sphere, Journal of Fluid Mechanics, 423,
385 33–69, https://doi.org/10.1017/S0022112000001701, 2000.

Gordon, G. L. and Marwitz, J. D.: An Airborne Comparison of Three PMS Probes, Journal of Atmospheric and Oceanic Technology, 1, 22–27, https://doi.org/10.1175/1520-0426(1984)001<0022:AACOTP>2.0.CO;2, 1984.

Hallett, J. and Mossop, S. C.: Production of Secondary Ice Particles during the Riming Process, Nature, 249, 26–28, https://doi.org/10.1038/249026a0, 1974.

390 Herzegh, P. H. and Hobbs, P. V.: Size Spectra of Ice Particles in Frontal Clouds: Correlations between Spectrum Shape and Cloud Conditions, Quarterly Journal of the Royal Meteorological Society, 111, 463–477, https://doi.org/10.1002/qj.49711146810, 1985.

Heymsfield, A. J., Bansemer, A., Field, P. R., Durden, S. L., Stith, J. L., Dye, J. E., Hall, W., and Grainger, C. A.: Observations and Parameterizations of Particle Size Distributions in Deep Tropical Cirrus and Stratiform Precipitating Clouds: Results from In

Situ Observations in TRMM Field Campaigns, Journal of the Atmospheric Sciences, 59, 3457–3491, https://doi.org/10.1175/1520-
395   0469(2002)059<3457:OAPOPS>2.0.CO;2, 2002.

Hobbs, P. V.: Ice Multiplication in Clouds, Journal of the Atmospheric Sciences, 26, 315–318, https://doi.org/10.1175/1520-
0469(1969)026<0315:IMIC>2.0.CO;2, 1969.

Hobbs, P. V. and Alkezweeny, A. J.: The Fragmentation of Freezing Water Droplets in Free Fall, Journal of the Atmospheric Sciences, 25,
881–888, https://doi.org/10.1175/1520-0469(1968)025<0881:TFOFWD>2.0.CO;2, 1968.

400   Hobbs, P. V. and Rangno, A. L.: Ice Particle Concentrations in Clouds, Journal of the Atmospheric Sciences, 42, 2523–2549,
https://doi.org/10.1175/1520-0469(1985)042<2523:IPCIC>2.0.CO;2, 1985.

Hogan, R. J., Field, P. R., Illingworth, A. J., Cotton, R. J., and Choularton, T. W.: Properties of Embedded Convection in Warm-Frontal
Mixed-Phase Cloud from Aircraft and Polarimetric Radar, Quarterly Journal of the Royal Meteorological Society, 128, 451–476,
https://doi.org/10.1256/003590002321042054, 2002.

405   Homann, H. and Bec, J.: Concentrations of Inertial Particles in the Turbulent Wake of an Immobile Sphere, Physics of Fluids, 27, 053 301,
https://doi.org/10.1063/1.4919723, 2015.

Houze, R. A., Hobbs, P. V., Herzegh, P. H., and Parsons, D. B.: Size Distributions of Precipitation Particles in Frontal Clouds, Journal of the
Atmospheric Sciences, 36, 156–162, https://doi.org/10.1175/1520-0469(1979)036<0156:SDOPPI>2.0.CO;2, 1979.

Huffman, P. J.: Supersaturation Spectra of AgI and Natural Ice Nuclei, Journal of Applied Meteorology (1962-1982), 12, 1080–1082, 1973.

410   Jenny, M. and Dušek, J.: Efficient Numerical Method for the Direct Numerical Simulation of the Flow Past a Single Light Moving Spherical
Body in Transitional Regimes, Journal of Computational Physics, 194, 215–232, https://doi.org/10.1016/j.jcp.2003.09.004, 2004.

Jenny, M., Dušek, J., and Bouchet, G.: Instabilities and Transition of a Sphere Falling or Ascending Freely in a Newtonian Fluid, Journal of
Fluid Mechanics, 508, 201–239, https://doi.org/10.1017/S0022112004009164, 2004.

Johnson, T. A. and Patel, V. C.: Flow Past a Sphere up to a Reynolds Number of 300, Journal of Fluid Mechanics, 378, 19–70,
415   https://doi.org/10.1017/S0022112098003206, 1999.

Koenig, L. R.: The Glaciating Behavior of Small Cumulonimbus Clouds, Journal of the Atmospheric Sciences, 20, 29–47,
https://doi.org/10.1175/1520-0469(1963)020<0029:TGBOSC>2.0.CO;2, 1963.

Korolev, A., Heckman, I., Wolde, M., Ackerman, A. S., Fridlind, A. M., Ladino, L. A., Lawson, R. P., Milbrandt, J., and Williams, E.: A
New Look at the Environmental Conditions Favorable to Secondary Ice Production, Atmospheric Chemistry and Physics, 20, 1391–1429,
420   https://doi.org/https://doi.org/10.5194/acp-20-1391-2020, 2020.

Kotouč, M., Bouchet, G., and Dušek, J.: Loss of Axisymmetry in the Mixed Convection, Assisting Flow Past a Heated Sphere, International
Journal of Heat and Mass Transfer, 51, 2686–2700, https://doi.org/10.1016/j.ijheatmasstransfer.2007.10.005, 2008.

Kotouč, M., Bouchet, G., and Dušek, J.: Transition to Turbulence in the Wake of a Fixed Sphere in Mixed Convection, Journal of Fluid
Mechanics, 625, 205, https://doi.org/10.1017/S0022112008005557, 2009.

425   Marshall, J. S. and Palmer, W. M. K.: The Distribution of Raindrops with Size, Journal of Meteorology, 5, 165–166,
https://doi.org/10.1175/1520-0469(1948)005<0165:TDORWS>2.0.CO;2, 1948.

Mossop, S. C.: The Origin and Concentration of Ice Crystals in Clouds, Bulletin of the American Meteorological Society, 66, 264–273,
https://doi.org/10.1175/1520-0477(1985)066<0264:TOACOI>2.0.CO;2, 1985.

Murphy, D. M. and Koop, T.: Review of the Vapour Pressures of Ice and Supercooled Water for Atmospheric Applications, Quarterly Journal
430   of the Royal Meteorological Society, 131, 1539–1565, https://doi.org/10.1256/qj.04.94, 2005.

Nix, N. and Fukuta, N.: Nonsteady-State Kinetics of Droplet Growth in Cloud Physics, Journal of the Atmospheric Sciences, 31, 1334–1343, https://doi.org/10.1175/1520-0469(1974)031<1334:NSKODG>2.0.CO;2, 1974.

Ormières, D., Provansal, M., Recherche, I. R. P. H. E. I. D., Hors, P., and Cnrs, U. M. R.: Transition to Turbulence in the Wake of a Sphere, Physical Review Letters, pp. 6–9, https://doi.org/10.1103/PhysRevLett.83.80, 1999.

435 Passarelli, R. E.: Theoretical and Observational Study of Snow-Size Spectra and Snowflake Aggregation Efficiencies, Journal of the Atmospheric Sciences, 35, 882–889, https://doi.org/10.1175/1520-0469(1978)035<0882:TAOSOS>2.0.CO;2, 1978.

Patade, S., Prabha, T. V., Axisa, D., Gayatri, K., and Heymsfield, A.: Particle Size Distribution Properties in Mixed-Phase Monsoon Clouds from in Situ Measurements during CAIPEEX, Journal of Geophysical Research: Atmospheres, 120, 10,418–10,440, https://doi.org/10.1002/2015JD023375, 2015.

440 Patera, A. T.: A Spectral Element Method for Fluid Dynamics: Laminar Flow in a Channel Expansion, Journal of Computational Physics, 54, 468–488, https://doi.org/10.1016/0021-9991(84)90128-1, 1984.

Prabhakaran, P., Weiss, S., Krekhov, A., Pumir, A., and Bodenschatz, E.: Can Hail and Rain Nucleate Cloud Droplets?, Physical Review Letters, 119, 128 701, https://doi.org/10.1103/PhysRevLett.119.128701, 2017.

Prabhakaran, P., Kinney, G., Cantrell, W., Shaw, R. A., and Bodenschatz, E.: Ice Nucleation in the Wake of Warm Hydrometeors, 445 arXiv:1906.06129 [physics], 2019.

Pruppacher, H. R. and Klett, J. D.: Microphysics of Clouds and Precipitation, Springer Netherlands, https://doi.org/10.1007/978-0-306-48100-0, 2010.

Rangno, A. L. and Hobbs, P. V.: Ice Particle Concentrations and Precipitation Development in Small Polar Maritime Cumuliform Clouds, Quarterly Journal of the Royal Meteorological Society, 117, 207–241, https://doi.org/10.1002/qj.49711749710, 1991.

450 Rønquist, E. M.: Optimal Spectral Element Methods for the Unsteady Three-Dimensional Incompressible Navier-Stokes Equations, Ph.D. thesis, Massachusetts Institute of Technology, 1988.

Schiller, L. and Naumann, A.: Über Die Grundlegenden Berechnungen Bei Der Schwerkraftaufbereitung, Z. Ver. Dtsch. Ing, 77, 318–320, 1933.

Takahashi, T., Nagao, Y., and Kushiyama, Y.: Possible High Ice Particle Production during Graupel–Graupel Collisions, Journal of the 455 Atmospheric Sciences, 52, 4523–4527, https://doi.org/10.1175/1520-0469(1995)052<4523:PHIPPD>2.0.CO;2, 1995.

Vardiman, L.: The Generation of Secondary Ice Particles in Clouds by Crystal–Crystal Collision, Journal of the Atmospheric Sciences, 35, 2168–2180, https://doi.org/10.1175/1520-0469(1978)035<2168:TGOSIP>2.0.CO;2, 1978.

Zhou, W. and Dušek, J.: Chaotic States and Order in the Chaos of the Paths of Freely Falling and Ascending Spheres, International Journal of Multiphase Flow, 75, 205–223, https://doi.org/10.1016/j.ijmultiphaseflow.2015.05.010, 2015.
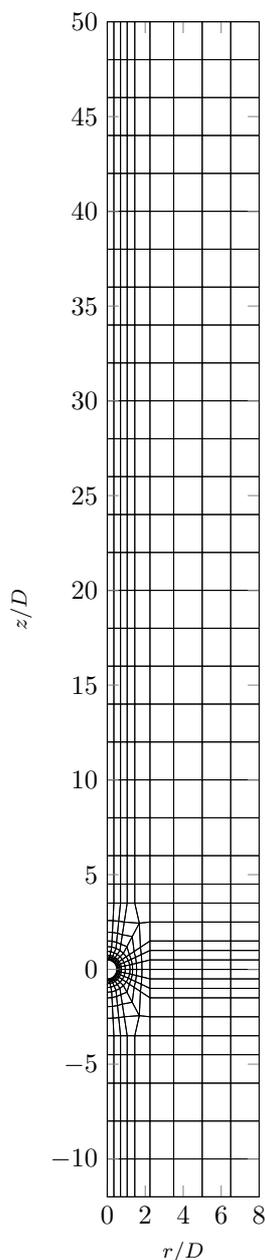
Figure 1. Spectral-element mesh in the axial-radial plane, where the lines depict the boundaries of the 463 elements. Each element contains $[6 \times 6]$ collocation points. The three-dimensionality is introduced by Fourier expansion in the azimuthal direction, which is truncated at the 7th Fourier mode, resulting in a cylindrical domain. A uniform velocity profile with constant temperature and vapor content is imposed at the upstream boundary, while the downstream boundary is subject to zero-gradient BCs for both velocity and scalars. The lateral boundaries are stress-free at zero pressure with zero-gradient BCs for the scalars. The surface of the spherical particle, whose center is located at the origin of the coordinate system, is impermeable and a no-slip BC for velocity is imposed as well as constant Dirichlet BCs for the scalar fields.
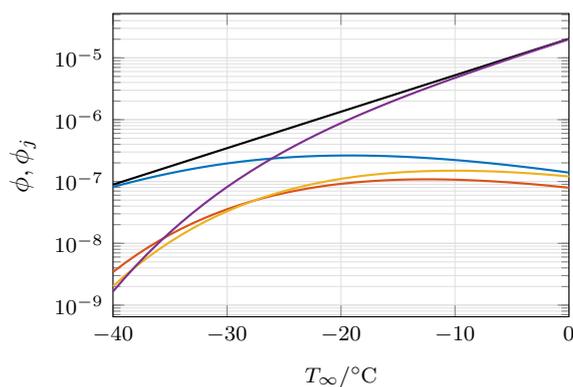
Figure 2. Volume fraction of ice particles in clouds as a function of ambient temperature. The total volume fraction ϕ is displayed by a solid black line (——), while the contribution by the regimes is given by the colored lines. Linestyles: axisymmetric regime (——), steady oblique regime (——), oscillating oblique regime (——), chaotic regime (——).
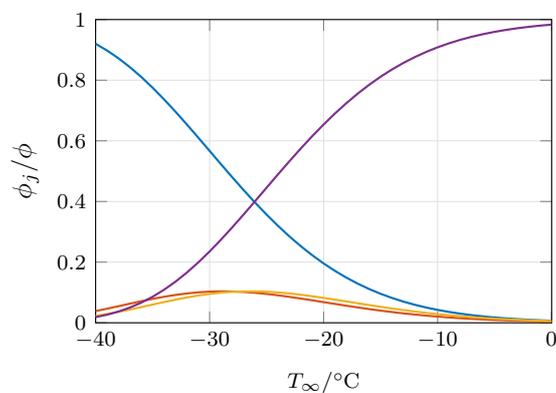
Figure 3. Relative contribution to the total volume fraction by hydrometeors in a certain regime. Linestyles: axisymmetric regime (——), steady oblique regime (——), oscillating oblique regime (——), chaotic regime (——).
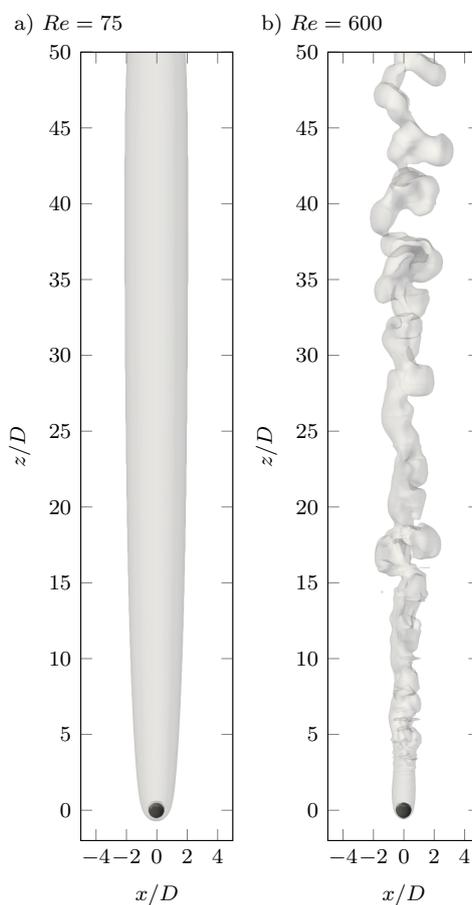
Figure 4. Isosurfaces of supersaturation in the wake at $T_\infty = -30°C$. The value of the isocontour is $\tilde{s}_i^* = 0.1$, i.e. ten percentage points higher than the ambient supersaturation. Two different wake regimes are depicted, which correspond to two different hydrometeor sizes in our framework. (a) axisymmetric regime at $Re = 75$, (b) chaotic regime at $Re = 600$.
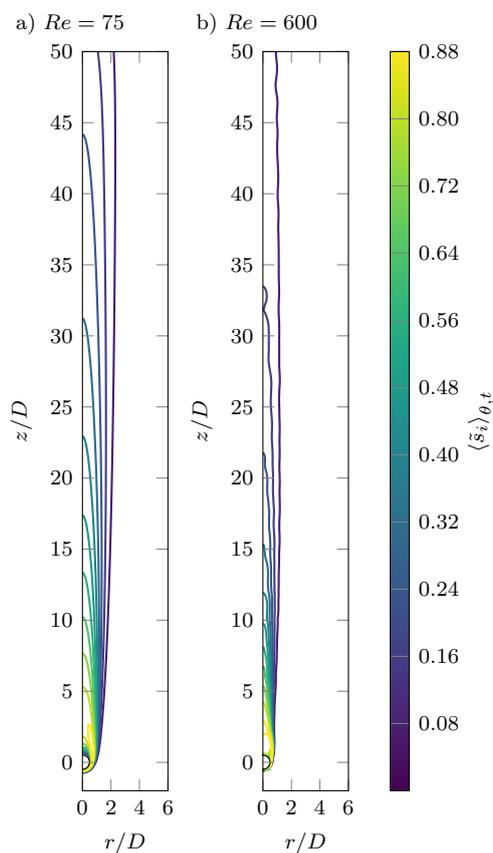
Figure 5. Contours of excess supersaturation in the wake, averaged over time and azimuthal direction at $T_\infty = -30°\text{C}$. (a) axisymmetric regime at $Re = 75$, (b) chaotic regime at $Re = 600$.
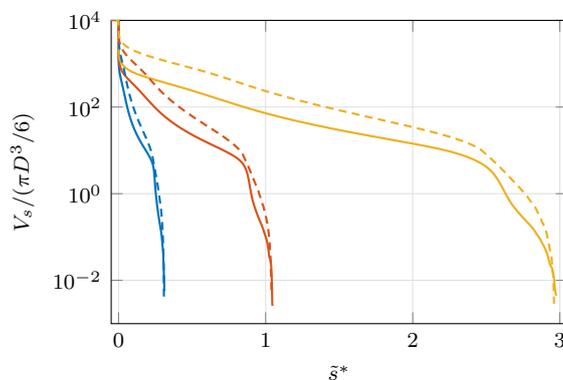
Figure 6. Volume of air where supersaturation exceeds a given threshold as a function of the threshold. The volume is normalized by the volume of the ice particle and three different temperatures are shown: $T_\infty = -20°\text{C}$ (——), $T_\infty = -30°\text{C}$ (——), $T_\infty = -40°\text{C}$ (——). Solid lines correspond to $Re = 600$ (chaotic regime), while dashed lines show the data obtained for $Re = 75$ (axisymmetric regime).
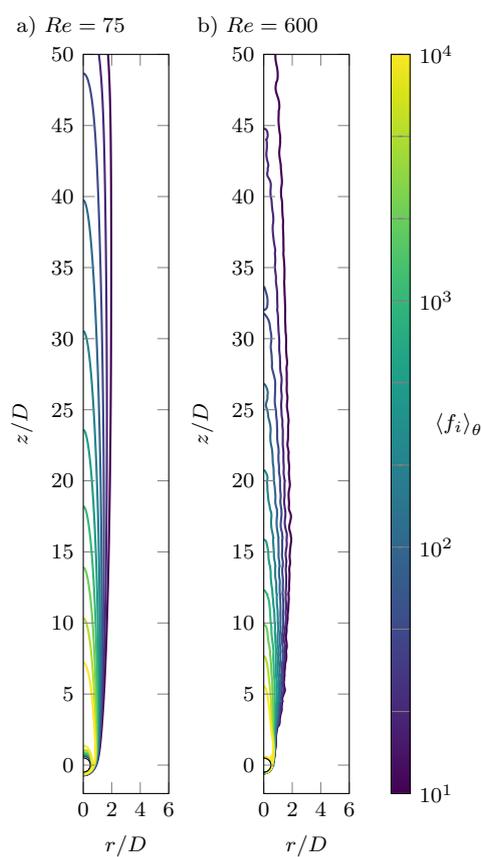
Figure 7. Contours of local ice enhancement factor in the wake, averaged over time and azimuthal direction at $T_\infty = -30°C$. The contour lines are spaced logarithmically. (a) axisymmetric regime at $Re = 75$, (b) chaotic regime at $Re = 600$.
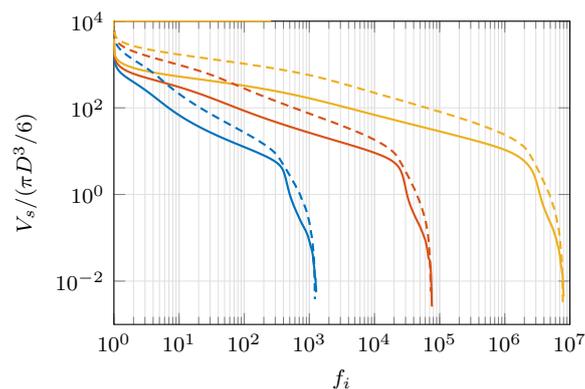
Figure 8. Volume of air with supersaturation above a given threshold as a function of the ice enhancement factor at $\alpha = 8$. The volume is normalized by the volume of the ice particle and three different temperatures are shown: $T_\infty = -20°C$ (——), $T_\infty = -30°C$ (——), $T_\infty = -40°C$ (——). Solid lines correspond to $Re = 600$ (chaotic regime), while dashed lines show the data obtained for $Re = 75$ (axisymmetric regime).
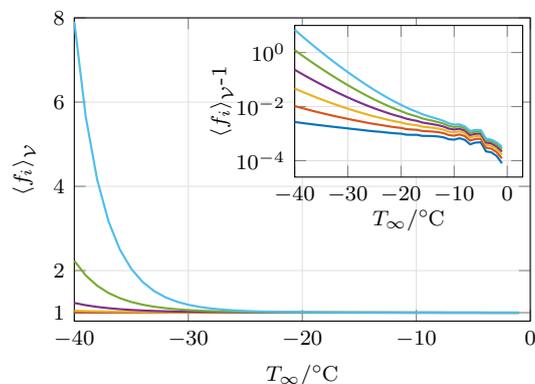
Figure 9. Global ice enhancement factor as a function of cloud temperature for various values of α. The inset shows the same data, but in semi-logarithmic scale. Linestyles: $\alpha = 3$ (——), $\alpha = 4$ (——), $\alpha = 5$ (——), $\alpha = 6$ (——), $\alpha = 7$ (——), $\alpha = 8$ (——).